Original Article

JCBFM

Journal of Cerebral Blood Flow & Metabolism
2017, Vol. 37(3) 1046–1059

DOI: 10.1177/0271678X16669514
journals.sagepub.com/home/jcbfm
SAGE

Effects of voluntary exercise on structure and function of cortical microvasculature

Adrienne Dorr[1,*], Lynsie AM Thomason[1,*], Margaret M Koletar[1], Illsung L Joo[1,2], Joe Steinman[2,3], Lindsay S Cahill[3], John G Sled[2,3] and Bojana Stefanovic[1,2]

Abstract

Aerobic activity has been shown highly beneficial to brain health, yet much uncertainty still surrounds the effects of exercise on the functioning of cerebral microvasculature. This study used two-photon fluorescence microscopy to examine cerebral hemodynamic alterations as well as accompanying geometric changes in the cortical microvascular network following five weeks of voluntary exercise in transgenic mice endogenously expressing tdTomato in vascular endothelial cells to allow visualization of microvessels irrespective of their perfusion levels. We found a diminished microvascular response to a hypercapnic challenge (10% $FiCO_2$) in running mice when compared to that in nonrunning controls despite commensurate increases in transcutaneous CO_2 tension. The flow increase to hypercapnia in runners was 70% lower than that in nonrunners ($p = 0.0070$) and the runners' arteriolar red blood cell speed changed by only half the amount seen in nonrunners ($p = 0.0085$). No changes were seen in resting hemodynamics or in the systemic physiological parameters measured. Although a few unperfused new vessels were observed on visual inspection, running did not produce significant morphological differences in the microvascular morphometric parameters, quantified following semiautomated tracking of the microvascular networks. We propose that voluntary running led to increased cortical microvascular efficiency and desensitization to CO_2 elevation.

Keywords

Exercise, two-photon microscopy, cerebral hemodynamics, brain imaging, cranial windows

Received 6 May 2016; Revised 7 July 2016; Accepted 31 July 2016

Introduction

Physical exercise can be a powerful tool for promoting brain health. Regular aerobic exercise has been shown to enhance performance on cognitive tasks in aged humans[1–6] and in learning and memory tests in animals.[7–13] In addition, physical exercise may be protective against Alzheimer's disease[8,9,14–20] and may enhance recovery from both stroke[21–25] and traumatic brain injury.[11] However, the changes in brain morphology and function underlying these effects remain incompletely understood.

Changes in cerebrovascular function in response to physical exercise may in part explain its beneficial effects on brain function. In aged humans who exhibit cerebral hypoperfusion,[26] regular exercise is associated with decreased blood pressure,[3,27] increased cerebral blood volume (CBV) in the hippocampus,[1] increased resting cerebral blood flow (CBF),[28–30] and increased cerebrovascular conductance.[3,30] Effects of exercise on blood flow increase to hypercapnia have been varied, with some studies showing higher cerebrovascular reactivity (CVR),[3,30–32] others showing decreased CVR,[29,31] and still others reporting no changes in CVR with exercise.[33] On the other hand, preclinical research has shown regionally specific increases in CBV and CBF in rodents,[1,34,35] with Swain et al. reporting increased vascular reactivity to hypercapnia in the motor cortex.[34]

[1]Sunnybrook Research Institute, Toronto, Canada
[2]Department of Medical Biophysics, University of Toronto, Toronto, Canada
[3]Mouse Imaging Centre, The Hospital for Sick Children, Toronto, Canada

*These authors contributed equally to this work.

Corresponding author:
Bojana Stefanovic, 2075 Bayview Avenue, room S6 56, Toronto, ON M4N 3M5, Canada.
Email: bojana@sri.utoronto.ca

In addition, age-related increases in oxidative stress have been shown to decrease with exercise in both humans[27] and rodents.[7,36] The antioxidative effects of exercise increase bioavailability of nitric oxide (NO),[24,25,36–40] which may be beneficial to the vasculature since low NO levels have been linked to vascular dysfunction.[27,41] Similarly, exercise induced increased expression of neuroprotective/antioxidant markers.[11,37]

Brain structural changes have also been observed. With exercise, humans exhibit gray and white matter volume increases,[2] increases in microvascular density, and decreased cerebrovascular tortuosity.[42] Experimental animals on exercise regimes have shown increases in brain volume and cortical thickness;[43–46] neurogenesis in the hippocampus;[1,10,13,47–49] and angiogenesis in the cortex,[34,50,51] hippocampus,[48,49] and cerebellum.[45,52,53] While rodent studies to date employed different forms of environmental enrichment in addition to an exercise wheel, it appears that the running component is the driving force at least for the neurogenesis and increased brain-derived neurotrophic factor (BDNF) peptide levels seen within the hippocampus.[54] Angiogenic and neurogenic effects of physical exercise take at least three days to present[49] and the elevated blood vessel density and neurogenesis are eventually extinguished after cessation of exercise.[12,49]

Notwithstanding, it has yet to be determined what brain functional hemodynamic changes occur at the microvascular level due to chronic exercise and how they may be coupled to morphological alterations in situ. Two-photon fluorescence microscopy (2PFM) provides an excellent way to image the hemodynamic changes at the micrometer scale. Bolus tracking and red blood cell (RBC) speed measurements during hypercapnia[55,56] can be performed with 2PFM to measure the vasodilatory response to CO_2 elevation at the microvascular level. In addition, high resolution 2PFM data on the mouse cortical microvascular architecture can be concomitantly acquired so as to assess exercise-induced changes in microvascular morphology. These assays were conducted presently to evaluate structural and functional changes in the cortical microvasculature following five weeks of voluntary exercise. We used Cre x tdTomato mice endogenously expressing tdTomato in vascular endothelial cells so as to assess angiogenesis at prelumen formation stages. Oregon Green dextran was injected intravascularly to measure bolus transit and RBC speed changes induced by hypercapnia.

Materials and methods

Animals

All experimental procedures in this study were approved by the Animal Care Committee of the Sunnybrook Health Sciences Center, which adheres to the Policies and Guidelines of the Canadian Council on Animal Care and meets all the requirements of the Provincial statute of Ontario, Animals for Research Act as well as those of the Federal Health of Animals Act. All animal experiments complied with the ARRIVE guidelines.[57] Thirty-five 12-week old Cre x tdTomato mice (B6.Cg-Tg(Tek-cre)1Ywa/JxB6; 129S6-Gt(ROSA)26Sortm14(CAG-tdTomato)Hze/J), bred in house, were used in this study: see Supplementary Table 1 for detailed description of animal allocation within study. These mice express tdTomato (a red fluorescent protein with an emission wavelength maximum of 581 nm) under the direction of the murine Tie2 promoter in endothelial cells.[58] Mice were randomly assigned into two groups: five weeks of voluntary exercise group ($n = 19$) and a nonrunning control group ($n = 16$). Three extra mice were assigned to the runner group to address lack of interest observed in prior work. Exercise mice had free access, within their standard cage, to a 5 in. inner diameter aluminum exercise wheel (Lafayette Instruments, Lafayette, IN, USA) affixed to the cage lid with an electronic odometer for daily readouts of the distance run. Additional animal enrichment included bedding (Aspen Sani-Chips, Harlan, Indianapolis, IN, USA), nestlets, and plastic mouse houses. Control mice were housed in the same conditions excluding the running wheel. Mice were allowed food and water ad libitum, with cages on ventilated racks and kept on a 12 h light/dark cycle with lights on at 7:00 am and off at 7:00 pm. Animal experimentation occurred during daytime light cycle following five weeks of voluntary running. Animals were euthanized by an overdose of sodium pentobarbital immediately following image acquisition. Four mice were lost to attrition: three died during the course of surgery and one died during image acquisition (cf. Supplementary Table 1).

Surgical preparation

Surgical procedures have been described in detail previously.[59,60] Briefly, mice (average weight ± standard deviation of 24 ± 4 g) were anesthetized via inhalation of isoflurane (5% induction; 1–2% maintenance). Body temperature was kept at 37.5°C using a heating pad, with feedback control input afforded by the rectal probe (TC-1000, CWE Inc., Ardmore, PA). Hydration was maintained with subcutaneous injections of 0.5–1.0 ml Ringer's solution. Animals were tracheostomized, mechanically ventilated (SAR 830/P, CWE Inc., Ardmore, PA) with 21% O_2 and balance nitrogen, and placed in a stereotaxic frame, with the head secured by ear and incisor bars. A circular cranial window, approximately 3 mm in diameter, was centered

over the primary motor cortex (1.75 mm medial–lateral and + 1.5 mm anterior–posterior relative to bregma). The cranial window was closed with a 5 mm circular glass coverslip (World Precision Instruments) secured to the surrounding skull with cyanoacrylate adhesive, and the dental cement-based well around the cranial window was filled with double distilled water for the water dipping objective. End tidal respiratory pressure and CO_2, transcutaneous CO_2, temperature, O_2 saturation, breath and pulse distension, and heart rate were recorded throughout surgery and imaging (Biopac MP150 Biopac Systems Inc., Goleta, CA; microcapstar CWE Inc., Ardmore, PA; TCM4 Radiometer, Copenhagen Denmark; MouseOx, Starr Life Sciences Corp, Oakmont, PA). Isoflurane was lowered to 1–1.25% during imaging. A gas mixer (GSM-3, CWE Inc.), triggered by the microscope image acquisition was used to deliver a mixture of 10% CO_2, 21% O_2, and balance nitrogen during 3–4 hypercapnic challenges that lasted at most 3 min, with an air-breathing period of 10 min between challenges.

Image acquisition

A tail vein catheter was implanted for the intravascular injection of fluorescent dextran (70 kDa Oregon green 33 mg/kg, dissolved in PBS; Invitrogen). In six animals, the tail vein catheterization failed, so Sulforhodamine 101 (SR101) was dissolved in PBS and injected intraperitoneally (10 mM solution, 8 µl/g) and line scans acquired as described below. The animal was placed in the stereotaxic frame with head secured by ear bars and an incisor bar. It was then positioned under a 25×1.05 NA objective with a working distance of 2 mm and a field of view of 509 µm × 509 µm (Olympus, Tokyo, Japan), with the animal and stage rotated to render the exposed cortical surface horizontal. Scanning was performed using a multiphoton laser scanning microscope (FV1000MPE Olympus, Tokyo, Japan). A Mai Tai mode-locked Titanium Sapphire tunable laser (690–1040 nm; Newport Corp, Irvine, CA) was used to excite the Oregon green dextran at 910 nm for bolus tracking scans, 900 nm for SR 101 line scans, and 985 nm for exciting both Oregon green and tdTomato during line scans and z-stacks. An external photomultiplier tube (Hamamatsu, Hamamatsu City, Japan) collected the resulting fluorescent emissions following bandpass filtering of 495/540 nm for Oregon green and 575/630 nm for tdTomato.

We performed three types of acquisitions. To estimate vascular transit times, four paired bolus injections of 30 µl (8.25 mg/kg, for a total of 33 mg/kg) of Oregon green were administered via the tail vein catheter during normocapnia and in the course of hypercapnia (10% CO_2 in the gas mixer delivered via GSM). A series of 2D frames were acquired during each bolus in a single transverse plane at 150 µm below the brain surface for the first pair and at 125 µm below the pial surface for the second pair, with 509 µm × 255 µm FOV, 2 µm × 2 µm nominal in-plane resolution, 2 µs/pixel, and ~230 ms/frame, for a total scan time of 60 s. To evaluate angiogenesis, z-stacks of 2D images parallel to the cortical surface were acquired between the pial surface and 300–700 µm below cortical surface, every 1.5 µm, with nominal in-plane resolution of 0.5–1.0 µm × 0.5–1.0 µm; and dwell time of 4–8 µs/pixel, for a total scan time of up to 45 min. Finally, paired line scans along the apparent centerlines of primary branches of cortical penetrating vessels were acquired to measure RBC velocities during normocapnia and hypercapnia. Each line scan comprised 10,000 lines acquired over ~12 s at 2 µs/pixel, ~1.2 ms/line, and a nominal spatial resolution of 0.5 µm/pixel.

Image analysis

All image segmentation was conducted by observers blinded to running and nonrunning groups. Maximum intensity projection (MIP) images were created with Imaris (Bitplane) software. Penetrating vessels were designated arterioles or venules based on their morphological features and branching pattern[61–64] as seen in the XYZ scans. Those cortical penetrating vessels exhibiting few branches across the imaged cortical depth, having a large capillary free space in their surround, and having a fairly constant diameter throughout their length were designated as arterioles. In turn, vessels showing more branches, a smaller capillary free space in their surround, and a diameter that progressively increased toward the cortical surface were deemed veins. Vessels with diameter less than 10 µm[65] not directly connected to a penetrating vessel were labeled as capillaries. Those vessels that did not have Oregon green dextran within their lumen but still showed tdTomato endothelial expression were designated as newly formed.

Automated vessel tracking, as described in Rennie et al.[66] and Ghanavati et al.[67] was performed on the Oregon Green perfused cortical vessels imaged in the z-stacks. This algorithm follows the centerlines of vessels, which are represented as discrete medial atoms.[68] The centerline is sampled every micrometer along the vessel by optimizing the position and radius of an image operator, which is defined by eight spokes extending from the atom to the vessel boundary, thus identifying centerline location, local tangent to the vessel, and vessel radius. The cost function optimized is the sum of the signal intensity gradients at the end of each spoke.

Each image was convolved with a 2D median filter (3 μm × 3 μm) and a 2D Gaussian blurring kernel with a full width at half maximum (FWHM) of 3 μm and then resampled to an isotropic voxel size of 1.5 μm × 1.5 μm × 1.5 μm. Tracing of vessels was initiated from numerous seed locations inside the vessels to enhance the likelihood of all vessels being traced. All voxels deemed within the foreground (based on manual signal thresholding) that were a local signal intensity maximum of the six nearest neighbors were selected as seed locations (to ensure most seeds were proximal to the centerlines of the vessels). To minimize computation time, tracking was not initiated in seeds located in a previously tracked vessel. The resulting graph was then used to gather data on morphological features of the microvasculature such as branch density, vessel density, diameter, length, and tortuosity. Figure 1(b) shows an example vessel-tracked data set. Three-dimensional rendering of vessel tracked data was created using Display (MINC tool kit, McConnel Brain Imaging Centre).

The bolus time series data acquired during normocapnia and hypercapnia were 2D median filtered (3 × 3 voxel kernel in x and y). MIP was performed on the filtered time series and the vessels of interest segmented semiautomatically. The average vessel signal intensity time series for each vessel in the imaging FOV was computed and normalized to the peak signal intensity of that vessel; the transit times were then analyzed across all vessels of the same vessel type (i.e. across all arterioles, capillaries, venules) on a population level. The bolus passage, during both normocapnia and hypercapnia, was next modeled using the gamma variate function,[69,70] as described previously.[55,71]

RBC speed estimates from line scans were calculated as described previously.[71] Data were filtered with a median filter (kernel size 2 × 2 pixels), followed by a Gaussian filter (kernel size 1 × 1 pixel) and the RBC speed then estimated using an algorithm based on Schaffer et al.[72]

Statistical analysis

All data were analyzed using linear mixed effects analysis (lme function in nlme package, R), with animals treated as random variables. This modeling yields sensible restricted maximum likelihood estimates from

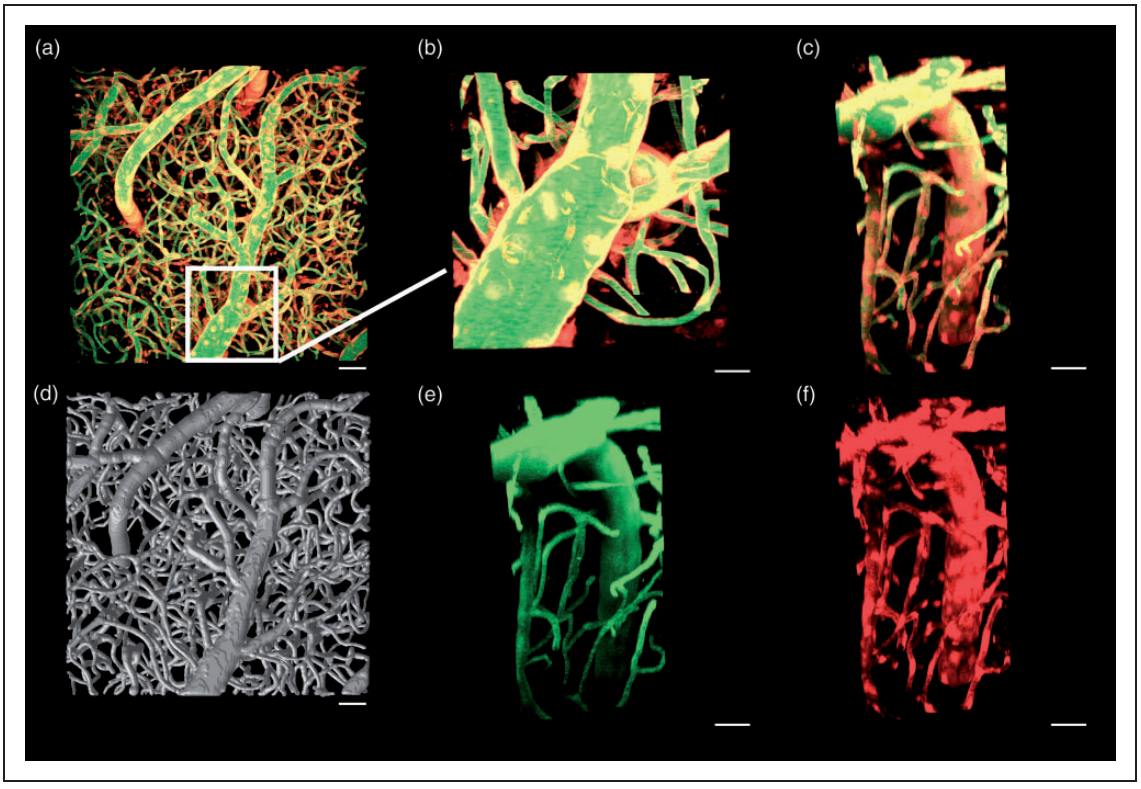

Figure 1. Maximum intensity projection normal to the cortical surface and centered over the primary motor cortex of a Cre x tdTomato mouse with vascular endothelial cells expressing tdTomato (red) and Oregon green dextran distributed within plasma (green) (a, scale 50 μm). The vessel-tracked vascular tree for this data set is seen in (d), scale 50 μm. Insets are of a penetrating vessel from the top (b, scale 20 μm) and the side showing the composite (c, scale 30 μm), green only (e, scale 30 μm), and red only (f, scale 30 μm) channel data.

unbalanced allocation of animals by factors presently resulting from attrition.[73] For vessel morphology measurements, average radius, length, and tortuosity were modeled as linear mixed effects functions of treatment (nonrunners, runners) and vessel type (arteriole, capillary, venule). For bolus tracking analysis, we modeled the time-to-peak (TTP) under hypercapnia as a linear function of two fixed effects: treatment (nonrunners, runners) and TTP under air breathing. We thereby evaluated the interaction between treatment and TTP under air on TTP under hypercapnia, so as to test for differences in slopes of TTP under hypercapnia versus TTP under air in runners versus nonrunners.[74] Compared to other slope comparison tests, linear mixed effects models have the advantage of accounting for within- and between-subject variation. The flow change was estimated from the inverse of the respective slope. Specifically, the decreased dispersion of TTP during hypercapnia relative to normocapnia under physiological conditions[56,59,75,76] was interpreted as a corresponding and proportionate increase in blood flow. For line scan data analysis, the change in arterial RBC speed induced by CO_2 challenge was modeled as a linear function of treatment.

Table 1. Systemic physiology of the runners and nonrunners.

	Distance ran (km/day)	SpO_2 (%)	Heart rate (bpm)	ΔtCO_2 (mmHg)
Nonrunner	N/A	96 ± 1	495 ± 11	11 ± 3
Runner	6.4 ± 0.8	96 ± 1	469 ± 12	15 ± 3

Arterial blood oxygenation (SpO_2 in %), heart rate (bpm), and change in transcutaneous CO_2 induced by hypercapnia. There were no significant differences between nonrunners and runners in any measures, but there was a trend of lower heart rate in the runners ($p = 0.12$). Mean ± SEM.

Results

No effects of running on systemic physiology or microvascular morphology

We observed no significant differences between runners and nonrunners with respect to their systemic physiology. In particular, heart rate, oxygen saturation at rest, and change in transcutaneous CO_2 induced by hypercapnia were not distinguishable between the two groups (Table 1).

Figure 1 shows MIP from an XYZ scan of a Cre x tdTomato nonrunner mouse. TdTomato expression provides a strong signal from the endothelium, while Oregon dextran distributes within plasma.

Figure 2 shows data from an example runner mouse: top (a) and side (b) MIP, as well as two example vessel segments found in layers II/III (indicated by blue arrows in (c) and (d)) not perfused with plasma, which may be newly formed vessels as we expect all mature capillaries to be perfused with plasma in a healthy brain.[76,77] (Similar evidence of angiogenesis has been reported using another endothelial–intravascular dye combination on 2PFM in the remodeling vascular tree of early postnatal brain and in hypoxia challenged adult mice.[78])

While the microvascular morphological parameters evaluated on the vessel tracked data agreed closely with

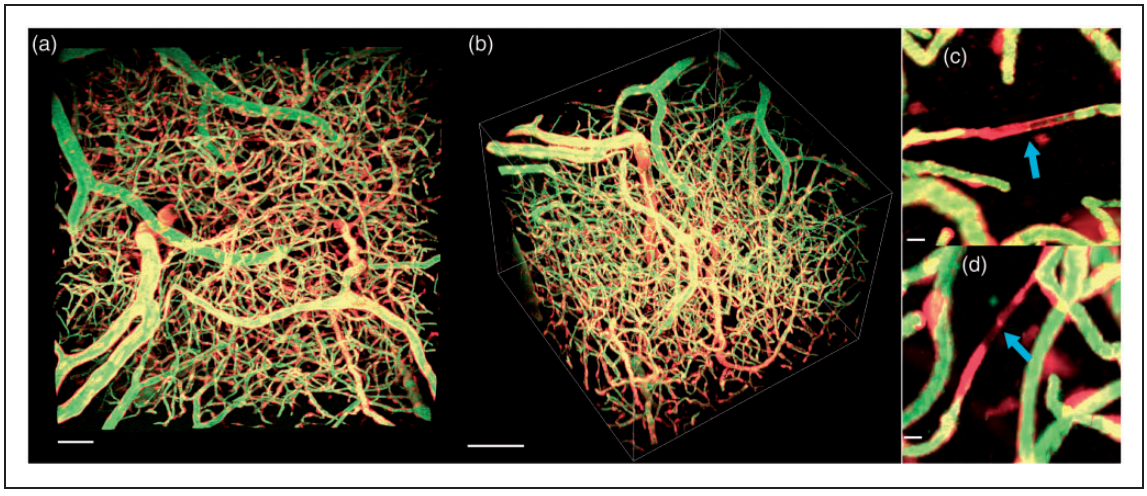

Figure 2. Maximum intensity projection of a two-photon fluorescence microscopy z-stack from the surface of the motor cortex (a, scale 50 μm) and side angle (b, scale 100 μm) with red showing vascular endothelial cells expressing tdTomato and green showing intravascular Oregon green. (c) and (d) (scale 10 μm) shows tdTomato labeling in the absence of Oregon green labeling (blue arrows), suggesting a new vessel.

previous literature[64,79–82] on the murine cortical microvasculature, there were no differences in runners versus nonrunners on any of the measured parameters (diameter, length, tortuosity, length density, vessel density, branch density, or vascular volume densities), consistent with the qualitative observations made by close visual inspection (Table 2). However, we did note a trend toward a ~7% decrease in the tortuosity of penetrating arterioles with running (runners: 1.09 ± 0.01; nonrunners: 1.18 ± 0.05; $p = 0.09$). Increased tortuosity of the brain vasculature has been observed in both healthy aging and in neurodegeneration in preclinical and clinical research and has been associated with cerebrovascular impairment in vivo,[59,83–85] so that decreased arteriolar tortuosity may be a morphological manifestation of increased vascular function or efficiency.

Attenuation of blood flow response to hypercapnia after voluntary exercise

To examine functional changes in cerebral vasculature induced by voluntary exercise, we followed the passage of a fluorescent dextran bolus through the microvascular bed at 125–150 μm beneath the cortical surface in 11 nonrunners and 11 runners. The signal peaked first in the artery, then in capillaries, and lastly in the veins (Figure 3(a) and (b) showing the signal time traces in a sample artery and a sample vein). Inhalation of 10% CO_2 induces a drop in pH and a robust cerebral (and peripheral) vasodilation and blood flow increase. Figure 3(c) and (d) shows signal traces in an example artery and vein from a nonrunner during air breathing (c) and during hypercapnia (d), showing the quickening of bolus transit through both vessels in response to hypercapnia. Similar changes are qualitatively observed in signal traces of an example artery and vein of a runner mouse, in Figure 3(e) (air breathing) and (f) (hypercapnia), but with an attenuated CO_2 induced shortening of arterial transit time. Due to the small lateral FOV and limited light penetration depth relative to the extent of mouse cortical cerebrovascular network, it is frequently not possible to ascertain whether a given pair of vessels are closely connected, precluding assessment of the effects of the vessel's branching order on the transit time.[86] Flow was estimated by inverse slope of Deming regression to hypercapnic versus normocapnic TTP data across all vessels (since no vessel-type effects were found), as shown in Figure 4. (Deming regression[87] minimizes the sum of distances in both the x and y, appropriate presently in light of errors on TTP estimates both during air breathing and during hypercapnia.) Runners exhibited a higher slope than did the nonrunners (0.78 ± 0.15 in runners versus 0.48 ± 0.18 in nonrunners; $p = 0.0070$), indicating a lower flow increase to hypercapnia in runners than in nonrunners. In particular, flow increased by a factor of 1.3 ± 0.2 in response to hypercapnia in runners and by a factor of 2.1 ± 0.8 in response to the same challenge in nonrunners. Of note, there was no difference in the hypercapnia-induced increase in transcutaneous CO_2 tension in these two groups ($p = 0.90$), suggesting that the observed attenuation of CVR was not secondary to peripheral adaptation.

Voluntary running-induced attenuation of arteriolar RBC speed increase to hypercapnia

Sample line scan data, acquired to allow estimation of RBC speeds, are shown in Figure 5. A section of the centerline of a primary branch of a penetrating vessel (Figure 5(a) and (b)) was imaged during both air (Figure 5(c)) and 10% CO_2 breathing (Figure 5(d)). No effect of running was seen on resting arteriolar RBC speed (2.4 ± 0.1 mm/s in runners ($N = 4$ mice); 2.3 ± 0.1 mm/s nonrunners ($N = 5$ mice); $p = 0.99$). Paralleling bolus tracking findings on hypercapnia-induced flow increases in the two cohorts, runners showed a smaller increase in RBC speed (0.44 ± 0.05 mm/s) in response to hypercapnia than

Table 2. Cortical microvasculature morphological characterization.

	Capillary	Penetrating arteriole	Penetrating venule	Nonpenetrating noncapillary
Vessel count per subject	820 ± 63	3.2 ± 0.3	7.5 ± 0.5	142 ± 25
Segment diameter (μm)	6.60 ± 0.11	12.25 ± 1.42	10.25 ± 0.68	13.45 ± 0.02
Segment length density (mm/mm^3)	566 ± 29	11 ± 1	27 ± 2	73 ± 14
Segment volume density (%)	1.99 ± 0.12	0.20 ± 0.04	0.24 ± 0.03	1.23 ± 0.03
Tortuosity	N/A	1.13 ± 0.03	1.11 ± 0.01	N/A
Branch density (branches/mm^3)	5633 ± 315			

Morphological characterization of the cortical microvascular networks imaged. The data from runners and nonrunners have been pooled due to absence of significant differences in any of the parameters examined. The average across-animal cortical vascular density was $3.5 \pm 0.3\%$. NA = not applicable. Mean ± SEM, N = 16 mice.

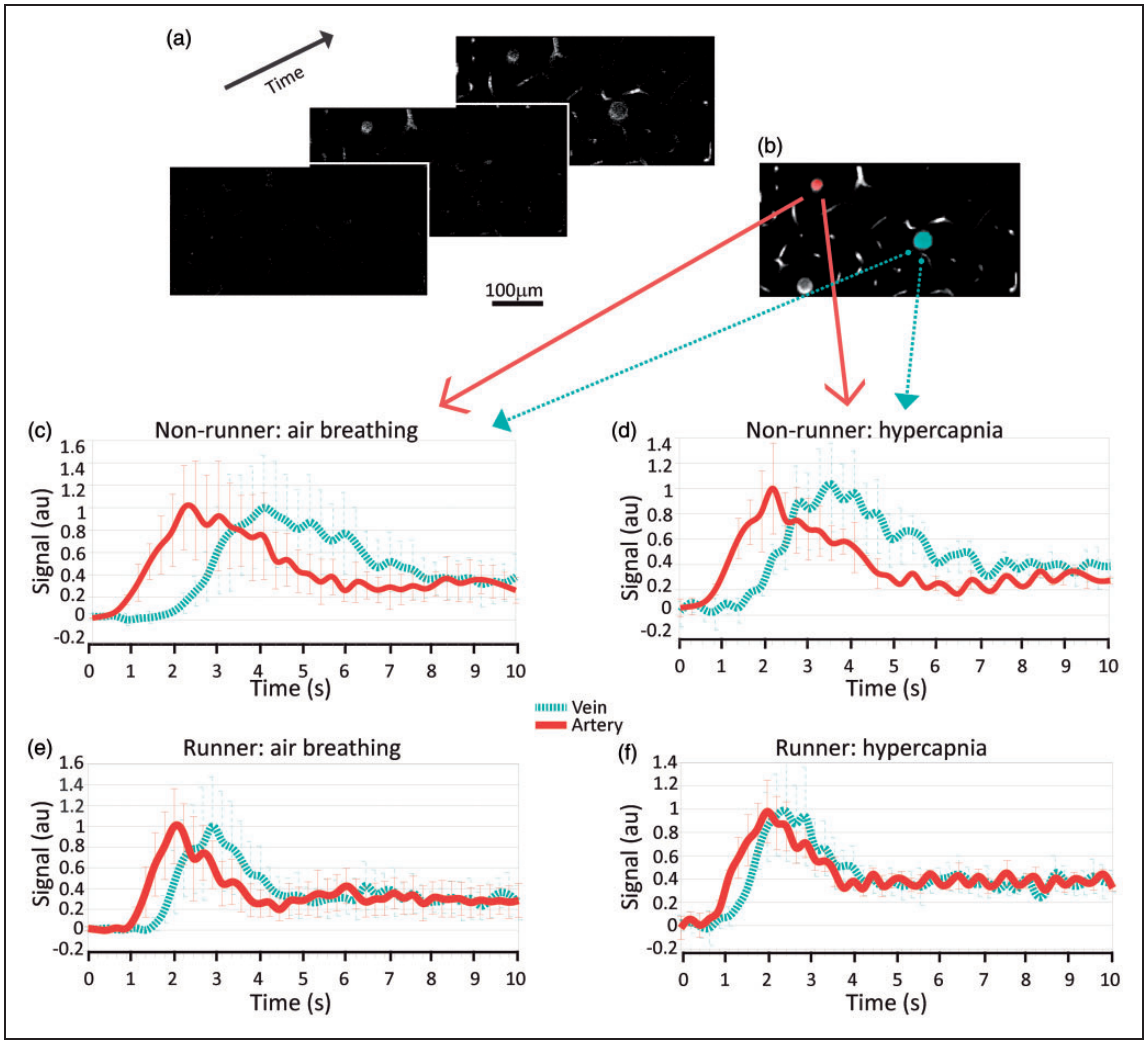

Figure 3. Samples of a bolus scan time series at a cortical depth of ~150 μm, showing the bolus arrival first in an artery (a, middle panel; b, red pseudocolor), then in capillaries, and lastly in a vein (a, last panel; b, blue pseudocolor). The mean fluorescence signal change over time in the artery (red) and in the vein (blue) during air (c) and hypercapnia (d) in a nonrunner mouse. The bolus transit is faster in the sample artery than in the sample vein in both conditions; the bolus transit is shortened in each vessel under hypercapnic mixture versus air breathing (mean ± stdev based on signal variation within the vessel). Artery: TTP = 2.28 ± 0.04 s during air, TTP = 1.84 ± 0.05 s during hypercapnia. Vein: TTP = 2.93 ± 0.30 s during air, TTP = 2.35 ± 0.04 s during hypercapnia. The mean signal change over time for an exercise mouse during air (e) and hypercapnia (f); bolus transit time during hypercapnia is shortened for the vein, but minimally affected for the artery. Artery: TTP = 2.00 ± 0.02 s during air, TTP = 1.78 ± 0.06 s during hypercapnia. Vein: TTP = 3.30 ± 0.05 s during air, TTP = 2.42 ± 0.07 s during hypercapnia.

did the nonrunners (0.85 ± 0.05 mm/s) (Figure 5(e)), by 0.45 ± 0.13 mm/s (p = 0.0085). Of note, however, in the animals for which arteriolar vRBC was evaluated, there was a trend toward smaller (by 8.3 ± 4.4 mmHg; p = 0.1) hypercapnia-induced increase in transcutaneous CO_2 in comparison to that of the nonrunning controls, suggesting that there may have been some differential effect on the periphery. In addition, runners showed a lower RBC speed increase across all vessels (N = 14 mice) with tCO_2 than did the nonrunners (N = 13 mice): runners: 0.0029 ± 0.0012 mm/s/mmHg; nonrunners: 0.014 ± 0.002 mm/s/mmHg (p = 1 e-5). Finally, runners exhibited decreased arteriolar RBC speed reactivity to tCO_2 elevation than did nonrunners: 0.021 ± 0.002 mm/s/mmHg (runners) versus 0.030 ± 0.002 mm/s/mmHg (nonrunners) (p = 0.0026). Ignoring a particularly avid runner (averaging 9 km/day versus 5–7 km/day for the rest), there was a trend toward lower arteriolar RBC speed during air breathing with increasing total distance ran (p = 0.08); and a trend toward lower arteriolar RBC speed during hypercapnia with increasing total distance

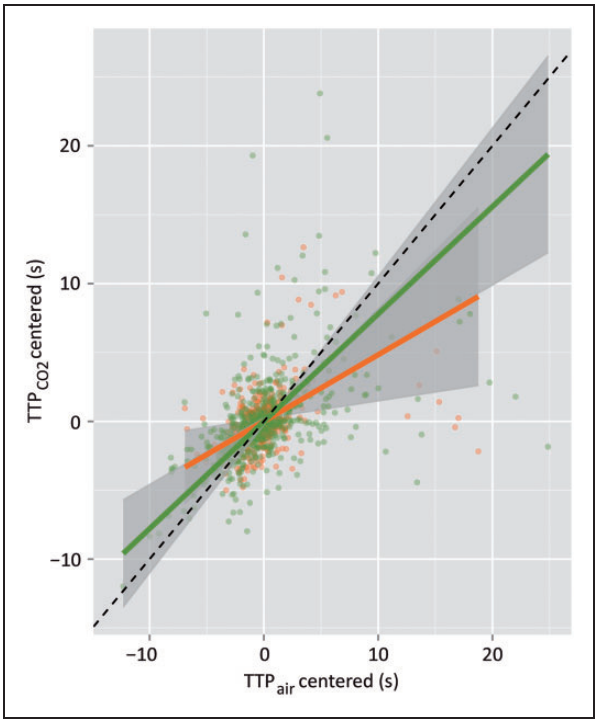

Figure 4. Scatterplot of the estimates of the time-to-peak intensity of the fluorescent signal over the course of the bolus passage in each scanned vessel during hypercapnic challenge (y-axis) versus that during air breathing (x-axis) (N = 11 runners, N = 11 nonrunners). The slope of the Deming regression to these data was 0.78 ± 0.15 in the runners (green line) and 0.48 ± 0.18 in the nonrunners (orange line). Flow change to hypercapnia was estimated by the inverse of the slope of the regression: flow thus increased in response to 10% CO_2 inhalation by a factor of 1.3 ± 0.2 in runners and by a factor of 2.1 ± 0.8 in nonrunners.

ran ($p = 0.10$), suggesting progressive increase in the system's efficiency (with respect to cerebral perfusion) with additional running, followed by eventual saturation of this effect (with extreme running). On the other hand, tCO_2 levels (during air or hypercapnic mixture breathing) were not affected by the distance ran ($p = 0.2$; $p = 0.4$ for air and hypercapnic conditions, respectively).

Discussion

In the present study, five weeks of voluntary running produced significant changes in the microvascular function in the primary motor cortex of mice. Whereas inhalation of 10% CO_2 doubled the cortical blood flow in nonrunners, it raised the flow in runners by only ~30%. Correspondingly, the RBC speed elevation in primary branches of cortical penetrating vessels of runners was only half that found in nonrunners. These reductions in hemodynamic responses to hypercapnia were not accompanied by significant changes in either microvascular network morphology or in systemic physiology, both assessed under anesthesia. We posit that the exercise regimen elevated the vascular reserve capacity[88] or network's efficiency, thus decreasing the challenge-induced perturbations of the existing microvascular network.

Voluntary exercise has shown a broad range of beneficial effects on systemic and central physiology in both preclinical models and humans[1,12,13,24,40,89] and has been promulgated as a promising therapeutic intervention to steady the effects of aging and neurodegeneration.[4,7,9,17,28,30,90,91] Exercise is thought to increase growth factor concentrations such as the neurogenesis impacting BDNF, the angiogenesis impacting vascular endothelial growth factor, and insulin-like growth factor 1 which influences both neurogenesis and angiogenesis.[47,51,53,54,92–96] Exercise upregulates NO production, which can influence the increase of BDNF production and improve cerebrovascular functionality.[25,35,39,97] Meanwhile chronic exercise regime has shown to decrease reactive oxidative species production and neuroinflammation, decreasing their negative effects on the above-mentioned growth factors and NO production.[7,27,36,96,98,99] Notwithstanding, the mechanisms underlying its many effects are not fully elucidated, hindering the rational design of exercise-based interventions.[96,100]

Brain microcirculation is a major target of exercise. To date, studies of the exercise-induced changes on brain vascular function have produced varied results, with regionally specific changes in cerebral vascular morphology and function. Autoradiographic measurements of CBF following six weeks of treadmill running in adult rats showed decreased perfusion in sensorimotor cortex—in agreement with current work—as well as in striatum, and vermis, but increased perfusion in deep cerebellar nuclei, thalamus, paravermis, and globus pallidus during slow walking on the Rotarod.[35] On the other hand, T2*-weighted MRI and flow-alternating inversion recovery MRI data acquired after 30 days of running in adult rats have indicated blood volume increases and a ~20% increase in motor cortical (relative to striatal) perfusion during 10% CO_2 breathing in rats.[34] CD61 integrin immunostaining in these animals also indicted capillary growth in motor cortex, with runners showing approximately doubled mean capillary volume fraction in layer II/III of the motor cortex.[34] In contrast, Kleim et al. found that 30 days of voluntary running in adult male rats resulted in increased blood vessel density in layer V of the forelimb motor cortex.[50] Limited light penetration in vivo precluded us from examining the microvascular morphology beyond layer III/IV in the present study. Notwithstanding, the current data on the cortical layers

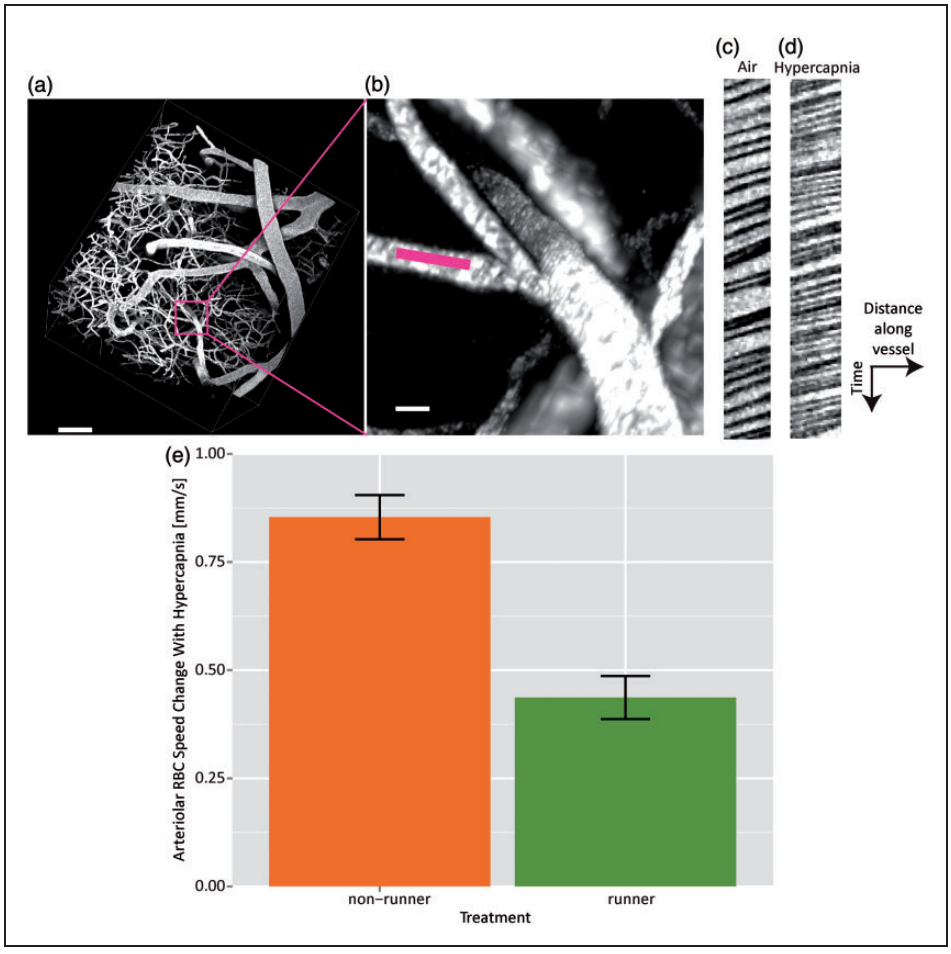

Figure 5. RBC speeds are measured in a penetrating vessel branch of an artery (a, scale 80 μm, and b, scale 10 μm, with pink line showing location of line scan). Line scan data samples from this vessel during air (c) and hypercapnia (d). RBC speeds thus estimated in this vessel were 1.32 ± 0.02 mm/s during air breathing and 1.86 ± 0.03 mm/s during breathing of 10% CO_2. Steeper slopes indicate smaller RBC speeds. Bar graph (e) showing change in arteriolar RBC speed induced by hypercapnia for nonrunners ($N = 5$) and runners ($N = 4$).

II/III provide evidence of the broader extent of functional changes relative to (any) morphological changes in the cerebral microvasculature induced by exercise. Future studies are required to examine effects of exercise on CVR in deeper cortical layers, using postmortem analysis or broader coverage in vivo techniques.

Directly comparing current observations to data from human studies is hindered by methodological confounds. Notwithstanding, in broad qualitative agreement with present observations, Thomas et al. showed higher baseline CBF with lower CO_2-induced CBF changes in elderly master athletes.[29] Gauthier et al. similarly reported lower CVR, as measured by BOLD fMRI, in frontal regions involved in the Stroop task processing in those elderly adults who performed the task faster and exhibited higher cardiorespiratory fitness.[31] Notwithstanding, investigations of the effects of exercise on the CVR in humans have yielded varied and region-specific findings.[3,29–33]

Anesthesia

The imaging was conducted under 1–1.25% isoflurane to ensure robust p_aCO_2 elevations; however, isoflurane exerts global vasodilatory effects.[101] In response to hypercapnia, the flow in nonrunners doubled, commensurate with prior observations in nonrunning mice under alpha-chloralose or propofol anesthesia[102–104] and suggesting ample dynamic range for flow regulation. Nonetheless, it is possible that the flow responses to hypercapnia would have been higher in awake animals,[105] supporting the acclimatization of animals to imaging procedures in future studies. However, awake imaging would likely confound hypercapnic challenges

(given respiratory adaptation[106,107]) and thus require use of alternate vasodilatory stimuli.

Degree of exercise

Our data suggest that the progressive decrease in hypercapnic reactivity seen with increased distance ran saturates at high level of running. Moreover, it is likely that extended exercise regimens eventually produce morphological changes in the cerebral microvasculature: Yoshihara et al. demonstrated increased capillary volume and surface area after 14 months of treadmill running in aged rats.[80]

Systemic effects

Chronic exercise regime in humans and animals is typically associated with decrease in resting blood pressure and a decrease in resting heart rate.[3,89,97,108,109] In light of methodological complexity of accurate blood pressure monitoring in mice, we have not tracked blood pressure in our animals in the present study. The heart rate measurements obtained during imaging experiments have not shown a difference between runners and nonrunners, though we did observe a trend toward decreased resting heart rate in runners, in agreement with the literature. Further, in the animals for which arteriolar RBC speed was measured, we have also seen a trend toward smaller hypercapnia-induced increase in transcutaneous CO_2 in runners when compared to nonrunners. On the whole, the present exercise regimen likely produced some, though limited systemic effects, in addition to the central effects described.

Cerebral vascular reserve capacity

On the level of both individual cortical vessels (interrogated by line scan measurements of vessel-wise RBC speeds) and the cortical microvascular network (studied by tracking the passage of the fluorescent bolus dextran), the present experiments indicate a reduced hemodynamic response to hypercapnia following the five weeks of ad lib running. Whereas decreased vascular reactivity is often interpreted as evidence of cerebrovascular dysfunction in disease,[59,110–113] we suggest that the present attenuation of the hemodynamic response to hypercapnia in runners may be a manifestation of increased efficiency of the system. In support of this notion, despite commensurate resting diameters, the dispersion in TTP was lower in runners than in nonrunners (ratio of variances of 1.6 ± 0.2, p-value < 1 e-5), another indicator of increased microvascular network efficiency. Although the preclinical evidence is limited,[35,114] there is mounting evidence in support of "neural efficiency" hypothesis, which suggests that significantly increased chronic utilization of a set of neuronal networks may raise the efficiency of their operation. In human studies, increased efficiency is most often reflected in decreased responses (both in terms of magnitude and spatial extent of changes) to task performance in experts. Thus, greater guitar playing skills correlate with decreased motor cortical activity (on EEG) during planning of motor movements involved in playing;[115] hemodynamic responses (on BOLD fMRI) in professional formula race car drivers are more focused than those in naïve drivers during performance of simple visuo-motor skill tasks;[116] compared to controls, skilled keyboard players show attenuated hemodynamic changes (on BOLD fMRI) in the cerebellum during complex finger movement tasks;[117] less cortical activity (on EEG) is seen in fitter than in less fit cyclists during cycling at the individual anaerobic threshold.[118]

In the context of current work, we postulate that chronic elevation of CO_2 levels during sustained exercise may lead to arteriolar desensitization to CO_2[29] as well as a metabolic adaptation leading to increased system's efficiency.[119] We speculate that NO signaling may be the mediator of the arteriolar desensitization given its involvement in hypercapnic vasodilation.[120,121] This hypothesis is motivated by prior demonstrations of exercise-induced increase in the availability of NO, which may induce short-term dilation,[38,122] followed by long-term desensitization of smooth muscle cells to NO elevations.[123] In addition to arteriolar desensitization to CO_2, we speculate that the chronic elevation in cortical activity as a result of exercise may also have led to the adaptation of the cortical metabolism, possibly by utilization of greater relative amounts of lactate-to-glucose[119] and hence allowing the brain to perform the same amount of "input processing" despite attenuated blood flow increase to the input stimulus and thus attenuated stimulation-induced increase in metabolite delivery. Future studies are required to examine the mechanisms of vascular desensitization and metabolic adaptation as a result of chronic voluntary exercise.

Conclusion

The present investigation provides evidence of attenuation in the CVR to hypercapnia in the primary motor cortex following five weeks of ad lib running in mice. The decrease in hypercapnia-induced changes occurred in the absence of any significant changes in the morphology of the cerebrovascular network or changes in the physiological monitoring parameters. The decrease in the flow response to hypercapnic challenge likely resulted from increased motor cortical efficiency and desensitization of the cortical arterioles to CO_2 manipulations.

Funding

The author(s) disclosed receipt of the following financial support for the research, authorship, and/or publication of this article: Canadian Institutes of Health Research Grant MOP 231389.

Acknowledgements

The authors would like to thank Jun Dazai for his technical assistance.

Declaration of conflicting interests

The author(s) declared no potential conflicts of interest with respect to the research, authorship, and/or publication of this article.

Authors' contribution

AD and LAMT contributed equally to this work. BS, JGS, and LSC designed the experiments. AD, LAMT, and MMK acquired the data. AD, LMAT, BS, ILJ, and JS analyzed the data. AD, LAMT, and BS wrote the manuscript. All authors reviewed and edited the manuscript.

Supplementary material

Supplementary material for this paper can be found at http://jcbfm.sagepub.com/content/by/supplemental-data

References

1. Pereira AC, Huddleston DE, Brickman AM, et al. An in vivo correlate of exercise-induced neurogenesis in the adult dentate gyrus. *Proc Natl Acad Sci USA* 2007; 104: 5638–5643.
2. Colcombe SJ, Erickson KI, Scalf PE, et al. Aerobic exercise training increases brain volume in aging humans. *J Gerontol* 2006; 61A: 5.
3. Brown AD, McMorris CA, Longman RS, et al. Effects of cardiorespiratory fitness and cerebral blood flow on cognitive outcomes in older women. *Neurobiol Aging* 2010; 31: 2047–2057.
4. Predovan D, Fraser SA, Renaud M, et al. The effect of three months of aerobic training on stroop performance in older adults. *J Aging Res* 2012; 2012: 269815.
5. Hayes SM, Alosco ML and Forman DE. The effects of aerobic exercise on cognitive and neural decline in aging and cardiovascular disease. *Curr Geriatr Rep* 2014; 3: 282–290.
6. Barnes JN. Exercise, cognitive function, and aging. *Adv Physiol Educ* 2015; 39: 55–62.
7. Navarro A, Gomez C, López-Cepero JM, et al. Beneficial effects of moderate exercise on mice aging: survival, behavior, oxidative stress, and mitochondrial electron transfer. *Am J Physiol Regul Integr Comp Physiol* 2004; 286: R505–R511.
8. Liu HL, Zhao G, Cai K, et al. Treadmill exercise prevents decline in spatial learning and memory in APP/PS1 transgenic mice through improvement of hippocampal long-term potentiation. *Behav Brain Res* 2011; 218: 308–314.
9. Adlard PA, Perreau VM, Pop V, et al. Voluntary exercise decreases amyloid load in a transgenic model of Alzheimer's disease. *J Neurosci* 2005; 25: 4217–4221.
10. Van Praag H, Shubert T, Zhao C, et al. Exercise enhances learning and hippocampal neurogenesis in aged mice. *J Neurosci* 2005; 25: 8680–8685.
11. Taylor JM, Montgomery MH, Gregory EJ, et al. Exercise preconditioning improves traumatic brain injury outcomes. *Brain Res* 2015; 1622: 414–429.
12. Rhyu IJ, Bytheway JA, Kohler SJ, et al. Effects of aerobic exercise training on cognitive function and cortical vascularity in monkeys. *Neuroscience* 2010; 167: 1239–1248.
13. Van Praag H, Christie BR, Sejnowski TJ, et al. Running enhances neurogenesis, learning, and long-term potentiation in mice. *Proc Natl Acad Sci USA* 1999; 96: 13427–13431.
14. Baker LDL and Frank L. Effects of aerobic exercise on mild cognitive impairment: a controlled trial. *Arch Neurol* 2010; 67: 71–79.
15. Larson EB, Wang L, Bowen JD, et al. Exercise is associated with reduced risk for incident dementia among persons 65 years of age and older. *Ann Intern Med* 2006; 144: 73–81.
16. Podewils LJ, Guallar E, Kuller LH, et al. Physical activity, APOE genotype, and dementia risk: findings from the Cardiovascular Health Cognition Study. *Am J Epidemiol* 2005; 161: 639–651.
17. Yuede CM, Zimmerman SD, Dong H, et al. Effects of voluntary and forced exercise on plaque deposition, hippocampal volume, and behavior in the Tg2576 mouse model of Alzheimer's disease. *Neurobiol Dis* 2009; 35: 426–432.
18. Ambrée O, Leimer U, Herring A, et al. Reduction of amyloid angiopathy and Aβ plaque burden after enriched housing in TgCRND8 mice. *Am J Pathol* 2006; 169: 544–552.
19. Herring A, Lewejohann L, Panzer A-L, et al. Preventive and therapeutic types of environmental enrichment counteract beta amyloid pathology by different molecular mechanisms. *Neurobiol Dis* 2011; 42: 530–538.
20. Lazarov O, Robinson J, Tang Y-P, et al. Environmental enrichment reduces Aβ levels and amyloid deposition in transgenic mice. *Cell* 2005; 120: 701–713.
21. Gao Y, Zhao Y, Pan J, et al. Treadmill exercise promotes angiogenesis in the ischemic penumbra of rat brains through caveolin-1/VEGF signaling pathways. *Brain Res* 2014; 1585: 83–90.
22. Lee HH, Kim H, Lee MH, et al. Treadmill exercise decreases intrastriatal hemorrhage-induced neuronal cell death via suppression on caspase-3 expression in rats. *Neurosci Lett* 2003; 352: 33–36.
23. Ding YH, Young CN, Luan X, et al. Exercise preconditioning ameliorates inflammatory injury in ischemic rats during reperfusion. *Acta Neuropathol* 2005; 109: 237–246.
24. Endres M, Gertz K, Lindauer U, et al. Mechanisms of stroke protection by physical activity. *Ann Neurol* 2003; 54: 582–590.
25. Gertz K, Priller J, Kronenberg G, et al. Physical activity improves long-term stroke outcome via endothelial nitric

oxide synthase-dependent augmentation of neovascularization and cerebral blood flow. *Circ Res* 2006; 99: 1132–1140.
26. Braz ID and Fisher JP. The impact of age on cerebral perfusion, oxygenation and metabolism during exercise in humans. *J Physiol* 2015; 594: 4471–4483.
27. Pialoux V, Brown AD, Leigh R, et al. Effect of cardiorespiratory fitness on vascular regulation and oxidative stress in postmenopausal women. *Hypertension* 2009; 54: 1014–1020.
28. Ainslie PN, Cotter JD, George KP, et al. Elevation in cerebral blood flow velocity with aerobic fitness throughout healthy human ageing. *J Physiol* 2008; 586: 4005–4010.
29. Thomas BP, Yezhuvath US, Tseng BY, et al. Life-long aerobic exercise preserved baseline cerebral blood flow but reduced vascular reactivity to CO_2. *J Magn Reson Imaging* 2013; 38: 1177–1183.
30. Bailey DM, Marley CJ, Brugniaux JV, et al. Elevated aerobic fitness sustained throughout the adult lifespan is associated with improved cerebral hemodynamics. *Stroke* 2013; 44: 3235–3238.
31. Gauthier CJ, Lefort M, Mekary S, et al. Hearts and minds: linking vascular rigidity and aerobic fitness with cognitive aging. *Neurobiol Aging* 2015; 36: 304–314.
32. Murrell CJ, Cotter JD, Thomas KN, et al. Cerebral blood flow and cerebrovascular reactivity at rest and during sub-maximal exercise: effect of age and 12-week exercise training. *Age (Omaha)* 2013; 35: 905–920.
33. Flück D, Braz ID, Keiser S, et al. Age, aerobic fitness and cerebral perfusion during exercise: role of carbon dioxide. *Am J Physiol Heart Circ Physiol* 2014; 307: 515–523.
34. Swain RA, Harris AB, Wiener EC, et al. Prolonged exercise induces angiogenesis and increases cerebral blood volume in primary motor cortex of the rat. *Neuroscience* 2003; 117: 1037–1046.
35. Holschneider DP, Yang J, Guo Y, et al. Reorganization of functional brain maps after exercise training: importance of cerebellar–thalamic–cortical pathway. *Brain Res* 2007; 1184: 96–107.
36. Durrant JR, Seals DR, Connell ML, et al. Voluntary wheel running restores endothelial function in conduit arteries of old mice: direct evidence for reduced oxidative stress, increased superoxide dismutase activity and down-regulation of NADPH oxidase. *J Physiol* 2009; 587: 3271–3285.
37. Chalimoniuk M, Jagsz S, Sadowska-krepa SJ, et al. Diversity of endurance training effects on antioxidant damage in different brain regions of adolescent male rats. *J Physiol Pharmacol* 2015; 4: 539–547.
38. Bolduc V, Thorin-Trescases N and Thorin E. Endothelium-dependent control of cerebrovascular functions through age: exercise for healthy cerebrovascular aging. *Am J Physiol Heart Circ Physiol* 2013; 305: H620–H633.
39. Pietrelli A, López-Costa JJ, Goñi R, et al. Effects of moderate and chronic exercise on the nitrergic system and behavioral parameters in rats. *Brain Res* 2011; 1389: 71–82.
40. Maeda S, Miyauchi T, Kakiyama T, et al. Effects of exercise training of 8 weeks and detraining on plasma levels of endothelium-derived factors, endothelin-1 and nitric oxide, in healthy young humans. *Life Sci* 2001; 69: 1005–1016.
41. Thomas SR, Witting PK and Drummond GR. Redox control of endothelial function and dysfunction: molecular mechanisms and therapeutic opportunities. *Antioxid Redox Signal* 2008; 10: 1713–1766.
42. Bullitt E, Rahman FN, Smith JK, et al. The effect of exercise on the cerebral vasculature of healthy aged subjects as visualized by MR angiography. *Am J Neuroradiol* 2009; 30: 1857–1863.
43. Cahill LS, Steadman PE, Jones CE, et al. MRI-detectable changes in mouse brain structure induced by voluntary exercise. *Neuroimage* 2015; 113: 175–183.
44. Huang CX, Qiu X, Wang S, et al. Exercise-induced changes of the capillaries in the cortex of middle-aged rats. *Neuroscience* 2013; 233: 139–145.
45. Isaacs KR, Anderson BJ, Alcantara AA, et al. Exercise and the brain: angiogenesis in the adult rat cerebellum after vigorous physical activity and motor skill learning. *J Cereb Blood Flow Metab* 1992; 12: 110–119.
46. Anderson BJ, Eckburg PB and Relucio KI. Alterations in the thickness of motor cortical subregions after motor-skill learning and exercise. *Learn Mem* 2002; 9: 1–9.
47. Fabel K, Fabel K, Tam B, et al. VEGF is necessary for exercise-induced adult hippocampal neurogenesis. *Eur J Neurosci* 2003; 18: 2803–2812.
48. Clark PJ, Brzezinska WJ, Puchalski EK, et al. Functional analysis of neurovascular adaptations to exercise in the dentate gyrus of young adult mice associated with cognitive gain. *Hippocampus* 2009; 19: 937–950.
49. Van Der Borght K, Kóbor-Nyakas DÉ, Klauke K, et al. Physical exercise leads to rapid adaptations in hippocampal vasculature: temporal dynamics and relationship to cell proliferation and neurogenesis. *Hippocampus* 2009; 19: 928–936.
50. Kleim JA, Cooper NR and VandenBerg PM. Exercise induces angiogenesis but does not alter movement representations within rat motor cortex. *Brain Res* 2002; 934: 1–6.
51. Ding Y-H, Li J, Zhou Y, et al. Cerebral angiogenesis and expression of angiogenic factors in aging rats after exercise. *Curr Neurovasc Res* 2006; 3: 15–23.
52. Black JE, Isaacs KR, Anderson BJ, et al. Learning causes synaptogenesis, whereas motor activity causes angiogenesis, in cerebellar cortex of adult rats. *Proc Natl Acad Sci USA* 1990; 87: 5568–5572.
53. Lopez-Lopez C, LeRoith D and Torres-Aleman I. Insulin-like growth factor I is required for vessel remodeling in the adult brain. *Proc Natl Acad Sci USA* 2004; 101: 9833–9838.
54. Kobilo T, Liu Q-R, Gandhi K, et al. Running is the neurogenic and neurotrophic stimulus in environmental enrichment. *Learn Mem* 2011; 18: 605–609.
55. Chinta LV, Lindvere L and Stefanovic B. Robust quantification of microvascular transit times via linear dynamical systems using two-photon fluorescence microscopy data. *J Cereb Blood Flow Metab* 2012; 32: 1718–1724.

56. Hutchinson EB, Stefanovic B, Koretsky AP, et al. Spatial flow-volume dissociation of the cerebral microcirculatory response to mild hypercapnia. *Neuroimage* 2006; 32: 520–530.
57. Kilkenny C, Browne WJ, Cuthill IC, et al. Improving bioscience research reporting: the ARRIVE guidelines for reporting animal research. *PLoS Biol* 2010; 8: e1000412.
58. Motoike T, Loughna S, Perens E, et al. Universal GFP reporter for the study of vascular development. *Genesis* 2000; 28: 75–81.
59. Dorr A, Sahota B, Chinta LV, et al. Amyloid-Beta-dependent compromise of microvascular structure and function in a model of Alzheimer's disease. *Brain* 2012; 135: 3039–3050.
60. Lindvere L, Janik R, Dorr A, et al. Cerebral microvascular network geometry changes in response to functional stimulation. *Neuroimage* 2013; 71: 248–259.
61. Scharrer E. Arteries and veins in the mammalian brain. *Anat Rec* 1940; 78: 173–196.
62. Duvernoy HMM, Delon S and Vannson JLL. Cortical blood vessels of the human brain. *Brain Res Bull* 1981; 7: 519–578.
63. Kasischke KA, Lambert EM, Panepento B, et al. Two-photon NADH imaging exposes boundaries of oxygen diffusion in cortical vascular supply regions. *J Cereb Blood Flow Metab* 2011; 31: 68–81.
64. Sugashi T, Yoshihara K, Kawaguchi H, et al. Automated image analysis for diameters and branching points of cerebral penetrating arteries and veins captured with two-photon microscopy. *Adv Exp Med Biol* 2014; 812: 209–215.
65. Santisakultarm TP, Cornelius NR, Nishimura N, et al. In vivo two-photon excited fluorescence microscopy reveals cardiac- and respiration-dependent pulsatile blood flow in cortical blood vessels in mice. *AJP Heart Circ Physiol* 2012; 302: H1367–H1377.
66. Rennie MY, Detmar J, Whiteley KJ, et al. Vessel tortuousity and reduced vascularization in the fetoplacental arterial tree after maternal exposure to polycyclic aromatic hydrocarbons. *Am J Physiol Heart Circ Physiol* 2011; 300: H675–H684.
67. Ghanavati S, Lerch JP and Sled JG. Automatic anatomical labeling of the complete cerebral vasculature in mouse models. *Neuroimage* 2014; 95: 117–128.
68. Fridman Y, Pizer SM, Aylward S, et al. Extracting branching tubular object geometry via cores. *Med Image Anal* 2004; 8: 169–176.
69. Kim J, Leira EC, Callison RC, et al. Toward fully automated processing of dynamic susceptibility contrast perfusion MRI for acute ischemic cerebral stroke. *Comput Methods Programs Biomed* 2010; 98: 204–213.
70. Kershaw LE and Cheng HLM. A general dual-bolus approach for quantitative DCE-MRI. *Magn Reson Imaging* 2011; 29: 160–166.
71. Stefanovic B, Hutchinson E, Yakovleva V, et al. Functional reactivity of cerebral capillaries. *J Cereb Blood Flow Metab* 2008; 28: 961–972.
72. Schaffer CB, Friedman B, Nishimura N, et al. Two-photon imaging of cortical surface microvessels reveals a robust redistribution in blood flow after vascular occlusion. *PLoS Biol* 2006; 4: 258–270.
73. Pinheiro JC and Bates DM. *Mixed-effects models in S and S-PLUS*. New York, NY: Springer Verlag, 2000.
74. Crawley MJ. Generalized linear models. In: *The R book*. Chichester, UK: John Wiley & Sons, Ltd, 2007, pp.511–526.
75. Abounader R, Vogel J and Kuschinsky W. Patterns of capillary plasma perfusion in brains in conscious rats during normocapnia and hypercapnia. *Circ Res* 1995; 76: 120–126.
76. Villringer A, Them A, Lindauer U, et al. Capillary perfusion of the rat brain cortex. An in vivo confocal microscopy study. *Circ Res* 1994; 75: 55–62.
77. Hudetz AG, Fehér G, Weigle CG, et al. Video microscopy of cerebrocortical capillary flow: response to hypotension and intracranial hypertension. *Am J Physiol* 1995; 268: H2202–H2210.
78. Harb R, Whiteus C, Freitas C, et al. In vivo imaging of cerebral microvascular plasticity from birth to death. *J Cereb Blood Flow Metab* 2013; 33: 146–156.
79. Heinzer S, Kuhn G, Krucker T, et al. Novel three-dimensional analysis tool for vascular trees indicates complete micro-networks, not single capillaries, as the angiogenic endpoint in mice overexpressing human VEGF165 in the brain. *Neuroimage* 2008; 39: 1549–1558.
80. Yoshihara K, Takuwa H, Kanno I, et al. Oxygen transport to tissue XIX. *Physiol Meas* 2009; 20: 293–298.
81. Wu J, He Y, Yang Z, et al. 3D BrainCV: simultaneous visualization and analysis of cells and capillaries in a whole mouse brain with one-micron voxel resolution. *Neuroimage* 2014; 87: 199–208.
82. Vogel J, Gehrig M, Kuschinsky W, et al. Massive inborn angiogenesis in the brain scarcely raises cerebral blood flow. *J Cereb Blood Flow Metab* 2004; 24: 849–859.
83. Lai AY, Dorr A, Thomason LAM, et al. Venular degeneration leads to vascular dysfunction in a transgenic model of Alzheimer's disease. *Brain* 2015; 138: 1046–1058.
84. Brown WR and Thore CR. Review: cerebral microvascular pathology in ageing and neurodegeneration. *Neuropathol Appl Neurobiol* 2011; 37: 56–74.
85. Moody DM, Brown WR, Challa VR, et al. Cerebral microvascular alterations in aging, leukoaraiosis, and Alzheimer's disease. *Ann NY Acad Sci* 1997; 826: 103–116.
86. Chinta LV, Lindvere L, Dorr A, et al. Quantitative estimates of stimulation-induced perfusion response using two-photon fluorescence microscopy of cortical microvascular networks. *Neuroimage* 2012; 61: 517–524.
87. Deming WE. *Statistical adjustment of data*. 1985th Dover Publications edition. New York: Wiley, 1943.
88. Davenport MH, Hogan DB, Eskes GA, et al. Cerebrovascular reserve: the link between fitness and cognitive function? *Exerc Sport Sci Rev* 2012; 40: 153–158.
89. Taddei S, Galetta F, Virdis A, et al. Physical activity prevents age-related impairment in nitric oxide availability in elderly athletes. *Circulation* 2000; 101: 2896–2901.
90. Wang S, Chen L, Zhang L, et al. Effects of long-term exercise on spatial learning, memory ability, and cortical capillaries in aged rats. *Med Sci Monit* 2015; 21: 945–954.

91. Colcombe SJ, Kramer AF, Erickson KI, et al. Cardiovascular fitness, cortical plasticity, and aging. *Proc Natl Acad Sci* 2004; 101: 3316–3321.
92. Trejo JL, Carro E and Torres-Aleman I. Circulating insulin-like growth factor I mediates exercise-induced increases in the number of new neurons in the adult hippocampus. *J Neurosci* 2001; 21: 1628–1634.
93. Carro E, Nuñez A, Busiguina S, et al. Circulating insulin-like growth factor I mediates effects of exercise on the brain. *J Neurosci* 2000; 20: 2926–2933.
94. Vaynman S, Ying Z and Gomez-Pinilla F. Hippocampal BDNF mediates the efficacy of exercise on synaptic plasticity and cognition. *Eur J Neurosci* 2004; 20: 2580–2590.
95. Neeper SA, Gómez-Pinilla F, Choi J, et al. Physical activity increases mRNA for brain-derived neurotrophic factor and nerve growth factor in rat brain. *Brain Res* 1996; 726: 49–56.
96. Cotman CW, Berchtold NC and Christie LA. Exercise builds brain health: key roles of growth factor cascades and inflammation. *Trends Neurosci* 2007; 30: 464–472.
97. Maeda S, Tanabe T, Otsuki T, et al. Moderate regular exercise increases basal production of nitric oxide in elderly women. *Hypertens Res* 2004; 27: 947–953.
98. Katusic ZS and Austin SA. Endothelial nitric oxide: protector of a healthy mind. *Eur Heart J* 2014; 35: 888–894.
99. Soto I, Graham LC, Richter HJ, et al. APOE stabilization by exercise prevents aging neurovascular dysfunction and complement induction. *PLoS Biol* 2015; 13: 1–33.
100. Gielen S, Schuler G and Adams V. Cardiovascular effects of exercise training: molecular mechanisms. *Circulation* 2010; 122: 1221–1238.
101. Cipolla M. Control of cerebral blood flow. In: Granger DN and Granger J (eds) *The cerebral circulation*. San Rafael, CA: Morgan & Claypool Life Sciences, 2009, pp.29–35.
102. Dalkara T, Irikura K, Huang Z, et al. Cerebrovascular responses under controlled and monitored physiological conditions in the anesthetized mouse. *J Cereb Blood Flow Metab* 1995; 15: 631–638.
103. Cenic A, Craen RA, Howard-Lech VL, et al. Cerebral blood volume and blood flow at varying arterial carbon dioxide tension levels in rabbits during propofol anesthesia. *Anesth Analg* 2000; 90: 1376–1383.
104. Franceschini MA, Radhakrishnan H, Thakur K, et al. The effect of different anesthetics on neurovascular coupling. *Neuroimage* 2010; 51: 1367–1377.
105. Sicard K, Shen Q, Brevard ME, et al. Regional cerebral blood flow and BOLD responses in conscious and anesthetized rats under basal and hypercapnic conditions: implications for functional MRI studies. *J Cereb Blood Flow Metab* 2003; 23: 472–481.
106. De Sanctis GT, Green FH and Remmers JE. Ventilatory responses to hypoxia and hypercapnia in awake rats pretreated with capsaicin. *J Appl Physiol* 1991; 70: 1168–1174.
107. Kinkead R, Dupenloup L, Valois N, et al. Stress-induced attenuation of the hypercapnic ventilatory response in awake rats. *J Appl Physiol* 2001; 90: 1729–1735.
108. Li N, Shi Y, Shi L, et al. Effects of aerobic exercise training on large-conductance Ca2+-activated K+ channels in rat cerebral artery smooth muscle cells. *Eur J Appl Physiol* 2013; 113: 2553–2563.
109. Adlam D, De Bono J, Danson E, et al. Telemetric analysis of haemodynamic regulation during voluntary exercise training in mouse models. *Exp Physiol* 2011; 96: 1118–1128.
110. Balbi M, Ghosh M, Longden TA, et al. Dysfunction of mouse cerebral arteries during early aging. *J Cereb Blood Flow Metab* 2015; 35: 1445–1453.
111. Leoni RF, Paiva FF, Henning EC, et al. Magnetic resonance imaging quantification of regional cerebral blood flow and cerebrovascular reactivity to carbon dioxide in normotensive and hypertensive rats. *Neuroimage* 2012; 58: 75–81.
112. Lacombe P, Oligo C, Domenga V, et al. Impaired cerebral vasoreactivity in a transgenic mouse model of cerebral autosomal dominant arteriopathy with subcortical infarcts and leukoencephalopathy arteriopathy. *Stroke* 2005; 36: 1053–1058.
113. Nur E, Kim Y, Truijen J, et al. Cerebrovascular reserve capacity is impaired in patients with sickle cell disease. *Blood* 2009; 114: 3473–3478.
114. Sampedro-Piquero P, Zancada-Menendez C, Begega A, et al. Effects of forced exercise on spatial memory and cytochrome c oxidase activity in aged rats. *Brain Res* 2013; 1502: 20–29.
115. Wright DJ, Holmes P, Di Russo F, et al. Reduced motor cortex activity during movement preparation following a period of motor skill practice. *PLoS One* 2012; 7: 1–9.
116. Bernardi G, Ricciardi E, Sani L, et al. How skill expertise shapes the brain functional architecture: an fMRI study of visuo-spatial and motor processing in professional racing-car and naïve drivers. *PLoS One* 2013; 8: 1–11.
117. Koeneke S, Lutz K, Wüstenberg T, et al. Long-term training affects cerebellar processing in skilled keyboard players. *Neuroreport* 2004; 15: 1279–1282.
118. Ludyga S, Gronwald T and Hottenrott K. The athlete's brain: cross-sectional evidence for neural efficiency during cycling exercise. *Neural Plast* 2016; Article ID 4583674.
119. Kemppainen J, Aalto S, Fujimoto T, et al. High intensity exercise decreases global brain glucose uptake in humans. *J Physiol* 2005; 568: 323–332.
120. Toda N, Ayajiki K and Okamura T. Cerebral blood flow regulation by nitric oxide. *Pharmacol Rev* 2009; 61: 62–97.
121. Thompson BG, Pluta RM, Girton ME, et al. Nitric oxide mediation of chemoregulation but not autoregulation of cerebral blood flow in primates. *J Neurosurg* 1996; 84: 71–78.
122. Kingwell BA. Nitric oxide-mediated metabolic regulation during exercise: effects of training in health and cardiovascular disease. *FASEB J* 2000; 14: 1685–1696.
123. De Kimpe SJ, Van Heuven-Nolsen D, van Amsterdam JG, et al. Induction of nitric oxide release by interferon-gamma inhibits vasodilation and cyclic GMP increase in bovine isolated mesenteric arteries. *J Pharmacol Exp Ther* 1994; 268: 910–915.